

Chemical and Lattice Stability of the Tin Sulfides

Jonathan M. Skelton,^{1*} Lee A. Burton,² Fumiyasu Oba,² and Aron Walsh^{1,3,4}

¹ Department of Chemistry, University of Bath, Claverton Down, Bath BA2 7AY, UK

² Laboratory for Materials and Structures, Institute of Innovative Research, Tokyo Institute of Technology, 4259 Nagatsuta, Midori-ku, Yokohama 226-8503, Japan

³ Department of Materials, Imperial College London, Exhibition Road, London SW7 2AZ, UK

⁴ Global E³ Institute and Department of Materials Science and Engineering, Yonsei University, Seoul 120-749, Korea

* Corresponding author; e-mail: j.m.skelton@bath.ac.uk

Abstract

The tin sulfides represent a materials platform for earth-abundant semiconductor technologies. We present a first-principles study of the five known and proposed phases of SnS together with SnS₂ and Sn₂S₃. Lattice-dynamics techniques are used to evaluate the dynamical stability and temperature-dependent thermodynamic free energy, and we also consider the effect of dispersion forces on the energetics. The recently identified π -cubic phase of SnS is found to be metastable with respect to the well-known orthorhombic *Pnma/Cmcm* equilibrium. The *Cmcm* phase is a low-lying saddle point between *Pnma* local minima on the potential-energy surface, and is observed as an average structure at high temperatures. Bulk rocksalt and zincblende phases are found to be dynamically unstable, and we show that whereas rocksalt SnS can potentially be stabilised under a reduction of the lattice constant, the hypothetical zincblende phase proposed in several earlier studies is extremely unlikely to form. We also investigate the stability of Sn₂S₃ with respect to SnS and SnS₂, and find that both dispersion forces and vibrational contributions to the free energy are required to explain its experimentally-observed resistance to decomposition.

Introduction

The tin sulfides are a technologically-important family of earth-abundant optoelectronic materials comprising tin monosulfide (SnS), tin disulfide (SnS_2) and tin sesquisulfide (Sn_2S_3). SnS has long been explored as a sustainable candidate photovoltaic (PV) absorber material.¹⁻³ SnS_2 is a two-dimensional semiconductor that can be exfoliated to give individual nano-sheets,⁴ and Sn_2S_3 is an example of a comparatively rare mixed-valence binary compound, possesses an unusual one-dimensional bonding structure,⁵ and is predicted to show ambipolar dopability.⁶

The Sn_xS_y system has a rich phase space.⁷ SnS is known to form several (meta)stable phases, which has led to a degree of uncertainty over which phase(s) are obtained under different growth conditions. There are currently five reported or proposed phases, *viz.* the ground-state orthorhombic *Pnma* phase,⁸ a high-temperature *Cmcm* phase,⁹ and three cubic phases - rocksalt,¹⁰ zincblende¹¹⁻¹³ and the recently-reported *P2_13* (“ π -cubic”) phase with a 64-atom primitive cell.¹⁴⁻¹⁷ The sesquisulfide Sn_2S_3 has also been a source of confusion, as it is relatively easy to prepare, and clearly distinguishable from the other tin sulphides,¹⁸ yet is frequently predicted to be unstable with respect to decomposition into SnS and SnS_2 in theoretical studies (e.g. as in the current Materials Project¹⁹ entry, mp-1509²⁰). Both issues are important for contemporary PV research, since not only are phase impurities highly likely to play a role in the underwhelming performance of current SnS -based devices,^{18, 21} but tin sulfides may also form as impurities during the growth of more complex multicomponent semiconductors such as $\text{Cu}_2\text{ZnSnS}_4$ (CZTS).²²

First-principles materials modelling, e.g. within the ubiquitous Kohn-Sham density-functional theory formalism,^{23, 24} affords a versatile means of exploring the subtleties of the equilibria between competing phases. However, to enumerate such a complex phase space, two common approximations made in contemporary modelling studies may need to be revisited, namely: (1) the poor description of weak dispersion interactions afforded by most generalised-gradient approximation (GGA) density functionals, which may be an issue in describing the sulfide phases with prominent non-bonding interactions;^{5, 25} and (2) the omission of vibrational contributions to the temperature-dependent free energy in thermodynamic models.^{26, 27} Consideration of the lattice dynamics would also

enable the assessment of the bulk dynamical stability of the different phases, providing important insight into which phases are likely or unlikely to form under typical growth conditions.

In this work, we address both issues through a consistent set of first-principles lattice-dynamics calculations on the five known and proposed phases of SnS together with SnS₂ and Sn₂S₃, performed using both the PBEsol GGA²⁸ and the dispersion-corrected²⁹ PBEsol + D3 functionals. We establish the dynamical and thermodynamic stability ordering of the competing SnS phases, and provide conclusive evidence that the various experimental reports of cubic SnS are likely to be the rocksalt or π -cubic phases rather than a zincblende polymorph. We also consider the thermodynamics of the decomposition of Sn₂S₃, and show that to predict its stability requires an accurate description of the weak interactions in its structure as well as accounting for the vibrational contributions to its free energy.

Computational methods

First-principles calculations were carried out using the pseudopotential plane-wave density-functional theory (DFT) formalism, as implemented in the Vienna *Ab initio* Simulation Package (VASP) code.³⁰

We performed calculations using the PBEsol functional²⁸ and PBEsol with the DFT-D3 dispersion correction²⁹ applied (i.e. PBEsol + D3). PBEsol was selected due to its being shown in a number of studies to provide a good description of the structural and vibrational properties of solids at a moderate computational cost.³¹⁻

³³

Initial models built from published crystal structures^{8, 9, 15, 34-37} were fully optimised to a tolerance of 10⁻² eV Å⁻¹ on the forces, using a plane-wave cutoff of 550 eV and carefully-converged **k**-point sampling (Table 1). A tight energy-convergence criterion of 10⁻⁸ eV was applied during the electronic minimisation. Projectoraugmented-wave (PAW) pseudopotentials^{38, 39} were used to model the core electrons, with the Sn 5s, 5p and 4d and the S 3s and 3p electrons being included in the valence shell.

System	Phonon Supercell (# Atoms)	k-points	
		Optimisation	Phonon
α -Sn	-	$12 \times 12 \times 12 \Gamma$ -MP	-
β -Sn	-	$16 \times 16 \times 32 \Gamma$ -MP	-
S	-	$3 \times 1 \times 1 \Gamma$ -MP	-
SnS (<i>Pnma</i>)	$6 \times 1 \times 6$ (384)	$8 \times 4 \times 8$ MP	$2 \times 4 \times 2$ MP
SnS (Cubic)	$2 \times 2 \times 2$ (512)	$2 \times 2 \times 2 \Gamma$ -MP	$1 \times 1 \times 1 \Gamma$ -MP
SnS (<i>Cmcm</i>)	$6 \times 1 \times 6$ (384)	$8 \times 4 \times 8$ MP	$2 \times 4 \times 2$ MP
SnS (Rocksalt)	$4 \times 4 \times 4$ (128)	$12 \times 12 \times 12 \Gamma$ -MP	$3 \times 3 \times 3 \Gamma$ -MP
SnS (Zincblende)	$4 \times 4 \times 4$ (128)	$8 \times 8 \times 8 \Gamma$ -MP	$2 \times 2 \times 2 \Gamma$ -MP
SnS ₂	$6 \times 6 \times 2$ (144)	$8 \times 8 \times 6 \Gamma$ -MP	$2 \times 2 \times 3 \Gamma$ -MP
Sn ₂ S ₃	$2 \times 4 \times 2$ (320)	$4 \times 8 \times 3 \Gamma$ -MP	$2 \times 2 \times 2 \Gamma$ -MP

Table 1 Phonon supercells and k-point sampling used for the geometry optimisations and supercell finite-displacement phonon calculations performed in this work (MP - Monkhorst-Pack mesh,⁴⁰ Γ -MP - Γ -centered MP mesh).

The PAW projection was performed in reciprocal space. Non-spherical contributions to the gradient corrections inside the PAW spheres were accounted for, and the precision of the charge-density grids was set automatically to avoid aliasing errors.

Lattice-dynamics calculations were performed on the optimised structures using the Phonopy package,^{41, 42} which was used to set up and post process supercell finite-displacement phonon calculations.⁴³ VASP was used as the force calculator, and an additional charge-density grid containing $8 \times$ the number of points as the standard one was used to evaluate the augmentation charges. The supercell expansions used to determine the second-order force-constant matrices are listed in Table 1. For all models apart from *Cmcm* SnS, the force constants were calculated in expansions of the primitive unit cells. The force constants for *Cmcm* SnS were calculated in an expansion of the conventional cell, and a transformation matrix to the primitive cell was applied when evaluating its phonon dispersion curves.

Phonon density of states (DoS) curves were obtained by interpolating the phonon frequencies onto a uniform $48 \times 48 \times 48$ Γ -centered \mathbf{q} -point mesh and using the linear tetrahedron method for the Brillouin-zone

integration. The phonon dispersions were obtained by interpolating the phonon frequencies along lines of \mathbf{q} -points passing between the high-symmetry points in the Brillouin zones of the primitive unit cells. Thermodynamic functions were computed from a set of phonon frequencies evaluated on the same $48 \times 48 \times 48$ \mathbf{q} -point grids as were used to obtain the phonon DoS curves.

Results & Discussion

Figure 1 shows the structures of the seven tin sulfide compounds examined in this study after structural optimisation with PBEsol.

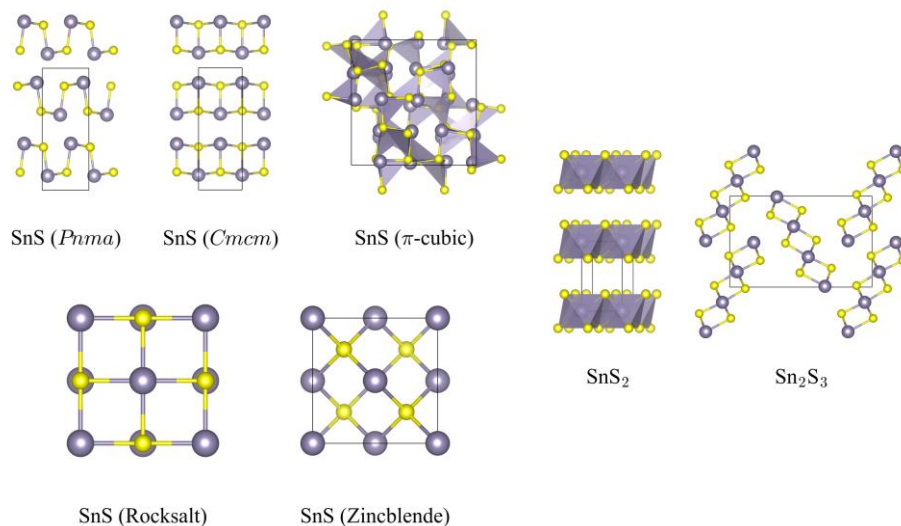


Figure 1 PBEsol-optimised structures of the *Pnma*, *Cmcm*, π -cubic, rocksalt and zincblende phases of SnS, SnS₂ and Sn₂S₃. These images were prepared using the VESTA software.⁴⁴

The structural diversity in the Sn_xS_y phase space is primarily driven by the ability of Sn to adopt two different oxidation states, *viz.* Sn(II) and Sn(IV).

The *Pnma*, *Cmcm* and π -cubic phases of SnS are built up from distorted Sn(II) tetrahedra with a stereochemically-active lone pair occupying one of the four coordination sites. The two orthorhombic phases are composed of layered 2D SnS sheets, with the lone pairs projecting into the interlayer space and facilitating a weak interaction along the crystallographic *b* axes. The low-temperature *Pnma* phase can be thought of as a small distortion of the more symmetric high-temperature *Cmcm* phase, and a phase transition between them occurs above 875 K.⁴⁵ The local coordination in the π -cubic phase is similar to that in the orthorhombic phases, but the Sn-S bonding in this structure instead forms a 3D network. In the higher-symmetry rocksalt and zincblende structures, the Sn lone pair must be accommodated within the close-packed structure, and the stability of this arrangement depends sensitively on the local chemical environment of the cation.⁴⁶

In SnS₂, symmetric edge-sharing Sn(IV) octahedra form 2D layers separated by a van der Waals' gap. Sn₂S₃ is a mixed oxidation-state phase containing equal proportions of Sn(II) and Sn(IV), and as such displays structural motifs from both SnS and SnS₂. The Sn₂S₃ structure consists of 1D chains of Sn(IV) octahedra capped by tetrahedral Sn(II), with weak interchain interactions facilitated by the Sn(II) lone pairs.

The optimised lattice parameters obtained with both exchange-correlation functionals (Table 2) were found to agree well with experimental measurements, and the PBEsol results were a good match to previous all-electron DFT calculations using the same functional.⁵ With the exception of zincblende SnS, the dispersion correction consistently yielded a smaller lattice volume, with a particularly notable contraction in the non-bonded *c* direction of SnS₂. The reduction in volume implies that the attractive part of the dispersion correction is dominant for most of the structures, whereas for the zincblende phase the dispersion correction produces a net repulsive effect. This can be explained by the interaction of the Sn(II) lone pair with the symmetric coordination environment: the Sn-S bond length in the rocksalt structure (PBEsol: 2.874 Å, PBEsol + D3: 2.856 Å) is considerably longer than in the zincblende structure (PBEsol: 2.778 Å, PBEsol + D3: 2.780 Å), which would lead to a stronger (repulsive) interaction between the lone pair and the bonding electrons.

The formation energies obtained with both functionals, referenced to solid S and β -Sn, are compared in Table 3. These values were used to draw a convex hull including the newly-discovered π -cubic phase (Figure 2).

	PBEsol			PBEsol + D3			Expt.		
	<i>a</i> [Å]	<i>b</i> [Å]	<i>c</i> [Å]	<i>a</i> [Å]	<i>b</i> [Å]	<i>c</i> [Å]	<i>a</i> [Å]	<i>b</i> [Å]	<i>c</i> [Å]
α -Sn	6.538	-	-	6.506	-	-	6.491 ³⁵	-	-
β -Sn	5.829	-	3.163	5.810	-	3.143	5.820 ³⁵	-	3.175 ³⁵
S	10.556	12.942	24.408	10.075	12.493	23.966	10.437 ³⁴	12.845 ³⁴	24.369 ³⁴
SnS (<i>Pnma</i>)	4.250	11.082	3.978	4.220	10.976	3.958	4.33 ⁸	11.18 ⁸	3.98 ⁸
SnS (Cubic)	11.506	-	-	11.405	-	-	11.603 ¹⁵	-	-
SnS (<i>Cmcm</i>) ^a	4.037	11.282	4.039	4.018	11.186	4.009	4.148 ⁹	11.480 ⁹	4.177 ⁹
SnS (Rocksalt)	5.747	-	-	5.712	-	-	-	-	-
SnS (Zincblende)	6.416	-	-	6.420	-	-	-	-	-
SnS ₂	3.651	-	6.015	3.639	-	5.721	3.638 ³⁶	-	5.880 ³⁶
Sn ₂ S ₃	8.811	3.766	13.813	8.633	3.760	13.663	8.878 ³⁷	3.751 ³⁷	14.020 ³⁷

Table 2 Optimised lattice constants of the models considered in this work obtained with the PBEsol and PBEsol + D3 exchange-correlation functionals. Experimental values are given where available for comparison. ^aThe lattice constants in Ref. 9 are reported at 905 K, and are therefore expected to include significant thermal expansion.

Both functionals predict the groundstate of SnS to be the *Pnma* phase, with the high-temperature *Cmcm* phase calculated to be 1.76 kJ mol⁻¹ per SnS formula unit (F.U.; PBEsol) and 1.63 kJ mol⁻¹ per F.U. (PBEsol + D3) higher in energy. The π -cubic phase is metastable with respect to this equilibrium, being 2.19 kJ mol⁻¹ per F.U. higher in energy with PBEsol, and 2.54 kJ mol⁻¹ per F.U. higher in energy with PBEsol + D3. The rocksalt phase is around 4× higher in energy than the π -cubic phase, at 8.54 kJ mol⁻¹ per F.U. with PBEsol and 10.75 kJ mol⁻¹ per F.U. with PBEsol + D3. The zincblende phase has a much smaller formation energy, and is thus very high in energy relative to all the other phases (PBEsol: 72.23 kJ mol⁻¹ per F.U., PBEsol + D3: 80.55 kJ mol⁻¹ per F.U.).

As in other calculations,^{6, 20} PBEsol predicts Sn₂S₃ to be above the convex hull, making it unstable with respect to decomposition into *Pnma* SnS and SnS₂.

System	E_F [kJ mol ⁻¹ per F.U.]			Bulk Dynamically Stable?
	PBEsol	PBEsol + D3	Expt.	
SnS (<i>Pnma</i>)	-90.59	-95.00	-100 to -108 ^{47, 48}	Yes
SnS (π -cubic)	-88.40	-92.46	-	Yes
SnS (<i>Cmcm</i>)	-88.83	-93.36	-	No
SnS (Rocksalt)	-82.05	-84.24	-	No
SnS (Zincblende)	-18.36	-14.45	-	No
SnS ₂	-120.00	-127.47	-148 to -182 ⁴⁸⁻⁵⁰	Yes
Sn ₂ S ₃	-208.90	-222.32	-249 to -297 ⁴⁸⁻⁵⁰	Yes

Table 3 Energetic and dynamical stability of the *Pnma*, π -cubic, *Cmcm*, rocksalt and zincblende phases of SnS, SnS₂ and Sn₂S₃. The calculated formation energies (E_F) of each compound are compared to experimental data where available, while the last column lists the bulk dynamical stabilities assessed from the harmonic phonon dispersions (see Figure 3).

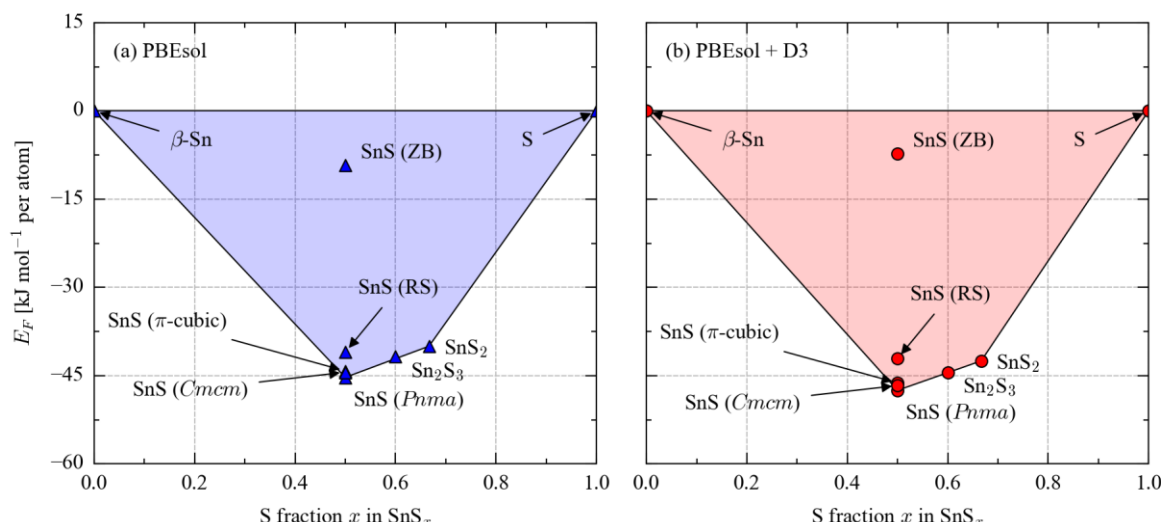


Figure 2 Thermodynamic convex hulls showing the calculated phase stability of the seven compounds in the Sn_xS_y system, based on formation energies obtained with (a) PBEsol and (b) PBEsol + D3. ZB and RS refer to the zincblende and rocksalt phases of SnS. The optimised crystal-structure parameters are reported in Table 2.

Whereas PBEsol predicts it to be 1.68 kJ mol⁻¹ above the hull, PBEsol + D3 predicts it to be much closer at 0.14 kJ mol⁻¹; this suggests that the dispersion correction selectively stabilises the sesquisulfide, most likely due to its improved description of the weak interactions between the bonded chains. Both values, but in particular the PBEsol + D3 one, are on the order of differences in the vibrational zero-point energy, a point which we return to below.

Finally, we note that the similar calculations carried out previously,⁵ although not including the π -cubic phase, were referenced to α -Sn; in the present calculations, both functionals predicted β -Sn to be lower in energy, but a similar comparison of the formation energies and a convex hull referenced to α -Sn yielded the same qualitative results (Table S1 and Figure S1 in the supporting information).

We next consider the dynamical stability of the seven sulfides. In the harmonic phonon model, displacement of atoms from their equilibrium positions along a normal-mode coordinate Q leads to a change in potential energy $U = \frac{1}{2}Q^2\omega^2$, where ω is the vibrational frequency. If a structure is a minimum on the potential-energy surface, U and ω are ≥ 0 (the three acoustic modes have $\omega = 0$ at the centre of the Brillouin zone (Γ)). If, on the other hand, a structure is a potential-energy maximum (e.g. a saddle point), atomic motion along one or more vibrations will lead to a lowering of the energy, and hence to a complex (imaginary) frequency.

In the present calculations, an analysis of the phonon dispersions (Table 1, Figure 3), that is, the frequencies of the $3N$ phonon bands as a function of the phonon wavevector, indicates the *Pnma* and π -cubic phases of SnS to be dynamically stable, whereas the *Cmcm*, rocksalt and zincblende phases all have imaginary modes.

The instability of the high-temperature *Cmcm* phase is anticipated, as the isostructural *Cmcm* phase of SnSe exhibits a similar phonon dispersion with imaginary modes at the same reciprocal-space wavevectors.⁵¹ The *Cmcm* structure is effectively a low-lying saddle point on the potential-energy surface, connecting equivalent distorted *Pnma* minima. Above the phase-transition temperature, sufficient thermal energy is available for the system to rapidly “hop” between the minima, and the higher-symmetry phase is observed as a crystallographic average structure with significant local distortions. The implication of this is that the *Cmcm* phase is only observed above the phase-transition temperature, and cannot be isolated under ambient conditions, e.g. by rapid quenching.

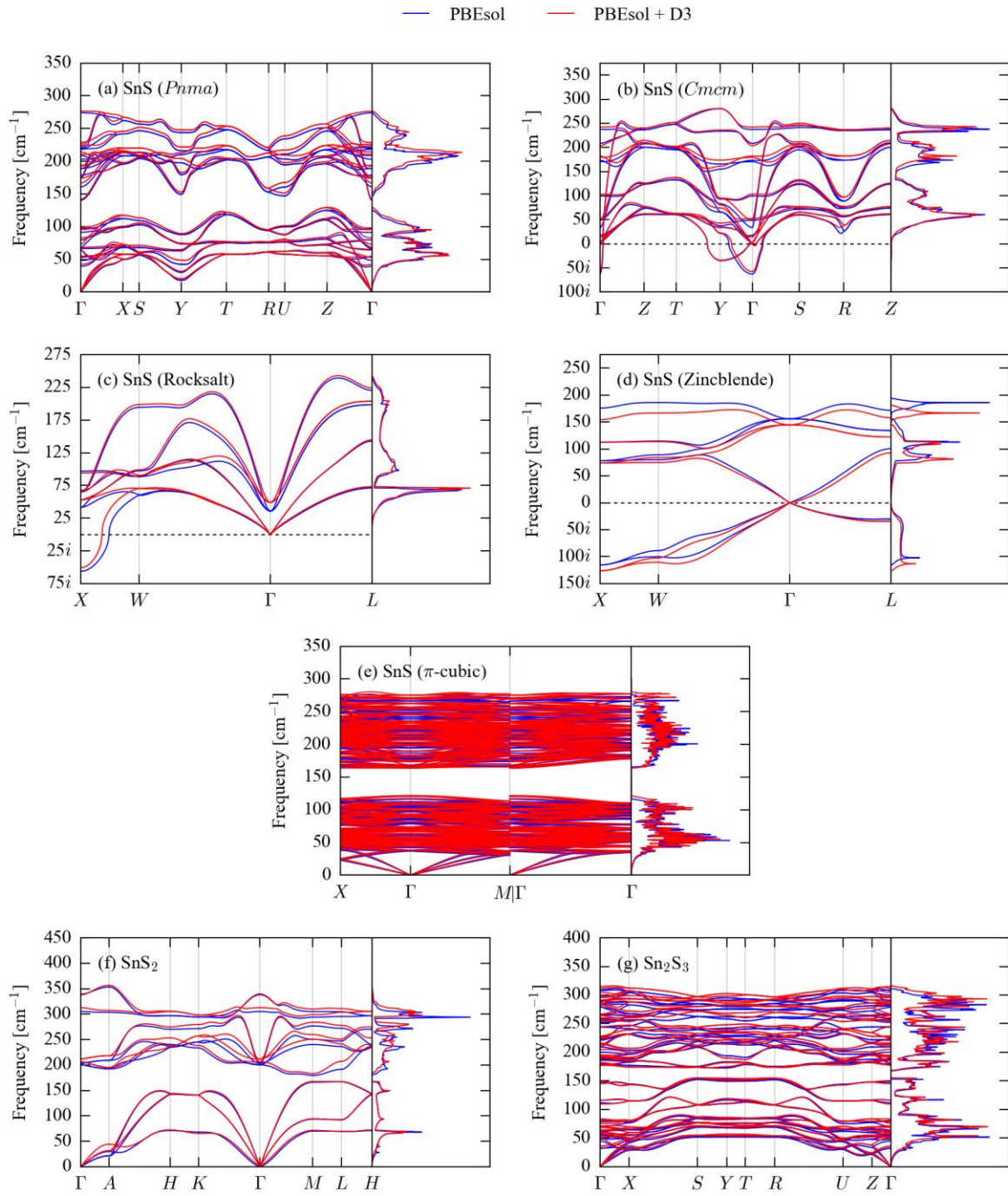


Figure 3 Phonon dispersion and density of states curves for the *Pnma* (a), *Cmcm* (b), rocksalt (c), zincblende (d) and π -cubic (e) phases of SnS, SnS₂ (f) and Sn₂S₃ (g), calculated within density-functional theory with electron exchange and correlation described by PBEsol (blue) and PBEsol + D3 (red).

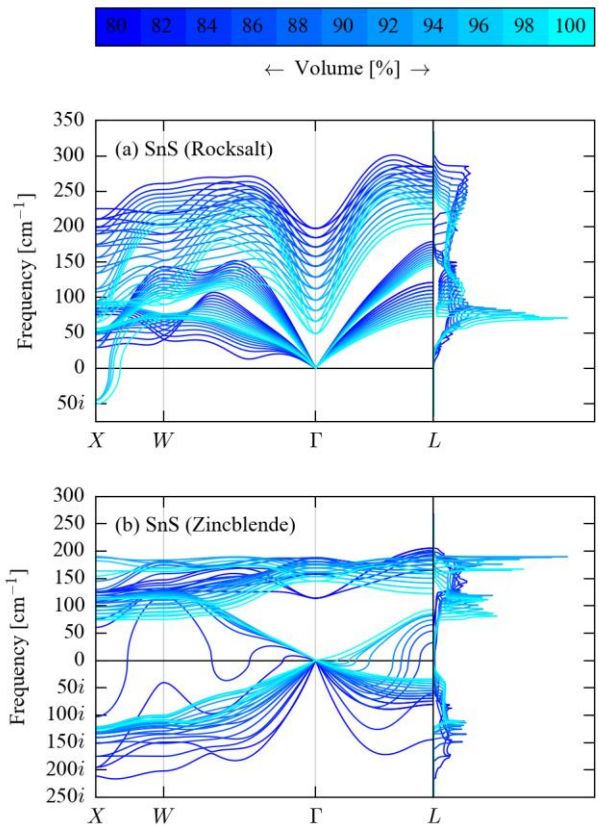


Figure 4 Phonon dispersion and density of states curves for the rocksalt (a) and zincblende (b) phases of SnS calculated at cell volumes ranging from the athermal equilibrium (cyan) to a 20 % compression (blue). Both sets of curves were computed with PBEsol + D3, and the results from identical calculations with PBEsol are presented in Figure S2 (supporting information).

The phonon instabilities in the rocksalt phase correspond to a fourfold enlargement of the two-atom primitive cell, suggesting a transition towards the *Pnma* phase. Whereas the imaginary modes in this structure (and also in the *Cmcm* phase) are restricted to well-defined phonon wavevectors and represent a small fraction of the overall phonon density of states (DoS), the zincblende instabilities account for a significant proportion ($\sim\frac{1}{3}$) of the integrated phonon DoS. Taken together with its predicted high formation energy, this phase is extremely unlikely to form, even under non-ambient conditions such as high pressure.

To confirm this, we calculated phonon dispersions of the rocksalt and zincblende phases for volume compressions of up to 20 %, corresponding to a 0.41-0.46 Å reduction in the lattice constants (Figure 4, see also Figure S2 in the supporting information). Under moderate compression, the imaginary modes in the rocksalt dispersion harden, indicating that the bulk phase can be dynamically stabilised under pressure. In contrast, compression of the zincblende phase was found to induce further phonon softening.

These results strongly suggest that cubic SnS has been misassigned as zincblende in various past studies. For example, the cubic lattice constant reported in Ref.¹³, 5.846 Å, is much closer to those of our rocksalt models (PBEsol: 5.747 Å, PBEsol + D3: 5.712 Å) than to those of our zincblende ones (PBEsol: 6.416 Å, PBEsol + D3: 6.420 Å). The rocksalt lattice constants are also a better match for the lattice constant of 6.00 Å measured for SnS films grown heteroepitaxially on NaCl. While it is possible that a rocksalt phase could be grown on certain substrates (or under pressure), we would argue that bulk cubic SnS is more likely to be the π -cubic phase, as: (1) our calculations show that this is dynamically stable in bulk; (2) the tetrahedral coordination environment in this structure is more likely to produce the tetrahedral morphology commonly observed in SnS nanoparticles;^{11, 16} and (3) it has been shown that the powder X-ray diffraction pattern of this phase may have been misinterpreted as that of a zincblende phase in the past.^{15, 17}

Both SnS_2 and Sn_3S_3 were found to be dynamically stable, as is expected given that these phases can be prepared as bulk single crystals.¹⁸

Comparing the phonon dispersion and DoS curves calculated using PBEsol and PBEsol + D3 reveals a general shift of the latter to higher frequencies due to the smaller predicted unit-cell volumes.³² The exception is zincblende SnS, where the slightly larger lattice constant predicted with PBEsol + D3 leads to a corresponding softening of the phonon frequencies. For all seven compounds, however, the main features, in particular the presence or absence of imaginary modes, are qualitatively similar.

As well as assessing dynamical stability, lattice-dynamics calculations also allow vibrational contributions to the free energy to be taken into account when assessing thermodynamic stability. Within the harmonic model, the constant-volume (Helmholtz) free energy, A , is given by:

$$A(T) = U_{\text{latt}} + U_{\text{vib}}(T) - TS_{\text{vib}}(T) \quad (1)$$

where U_{latt} is the (athermal) lattice energy (i.e. the total energy calculated using DFT, in the present study), U_{vib} is the vibrational internal energy, and S_{vib} is the vibrational entropy. $A(T)$ is typically evaluated from the lattice energy and phonon frequencies using the bridge relation from statistical mechanics:

$$\begin{aligned} A(T) &= -k_B T \ln Z(T) \\ &= U_{\text{latt}} + \frac{1}{N} \left\{ \frac{1}{2} \sum_{\mathbf{q}\nu} \hbar\omega(\mathbf{q}\nu) + k_B T \sum_{\mathbf{q}\nu} \ln \left[1 - e^{\frac{-\hbar\omega(\mathbf{q}\nu)}{k_B T}} \right] \right\} \end{aligned} \quad (2)$$

where $Z(T)$ is the thermodynamic partition function, k_B is Boltzmann's constant, the phonon frequencies ω are indexed by a reciprocal-space wavevector \mathbf{q} and a band index ν , and the sum over the phonon Brillouin zone is normalised by the number of unit cells in the crystal, N , equivalent to the number of wavevectors included in the summation.

The Helmholtz energies of the *Cmcm*, π -cubic and rocksalt phases of SnS, relative to the *Pnma* phase, are shown as a function of temperature in Figure 5, and free-energy differences calculated at 0, 300 and 900 K are listed in Table 4.

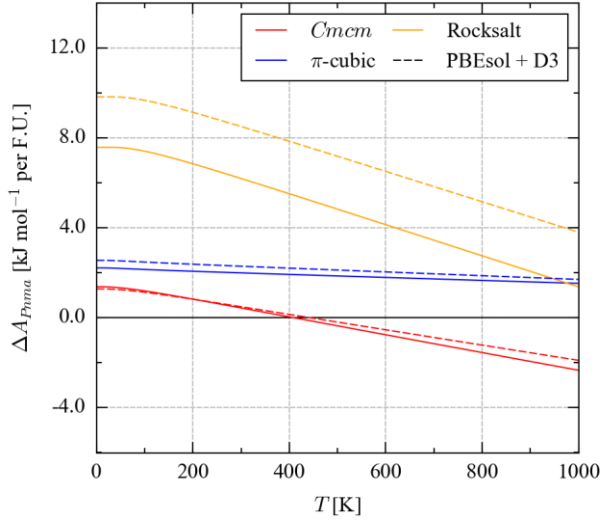


Figure 5 Thermodynamic stability of the *Cmcm* (red), π -cubic (blue) and rocksalt (yellow) phases of SnS, as a function of temperature, relative to the low-temperature groundstate *Pnma* phase, based on the constant-volume (Helmholtz) free energies, A , calculated with PBEsol (solid lines) and PBEsol + D3 (dashed lines).

[kJ mol ⁻¹ per F.U.]							
	PBEsol				PBEsol + D3		
	ΔU_{latt}	$\Delta A_{0\text{K}}$	$\Delta A_{300\text{K}}$	$\Delta A_{900\text{K}}$	ΔU_{latt}	$\Delta A_{0\text{K}}$	$\Delta A_{300\text{K}}$
<i>Pnma</i>	0.00	0.00	0.00	0.00	0.00	0.00	0.00
Cubic	2.19	2.23	2.01	1.61	2.54	2.56	2.30
<i>Cmcm</i>	1.76	1.39	0.45	-1.93	1.63	1.29	0.49
Rocksalt	8.54	7.63	6.24	2.11	10.75	9.85	8.53
Zincblende	72.23	-	-	-	80.55	-	-

Table 4 Relative energies of the five phases of SnS compared to the groundstate *Pnma* phase. The lattice energies, ΔU_{latt} , and constant-volume (Helmholtz) free energies, ΔA , at 0, 300 and 900 K calculated with PBEsol and PBEsol + D3 are compared. Energies are given in kJ mol⁻¹ per SnS formula unit. Due to the large proportion of imaginary phonon modes in its phonon density of states, we did not calculate free energies for the zincblende phase.

Although, as noted above, the high-temperature *Cmcm* phase is an average structure, since the imaginary modes form a small part of the overall phonon DoS we make the approximation that the static configuration provides a reasonable representation of its (average) internal energy and lattice dynamics. Doing so predicts the free energies of the *Pnma* and *Cmcm* phases to cross at around 400-450 K, which, although qualitatively correct, is considerably lower than the 875 K at which the phase transition is observed experimentally. This can be ascribed to the approximations made in the present calculations, including the approximate treatment of the physics of the phase transition, and possibly also the neglect of volume expansion and other forms of anharmonicity.⁵¹

The π -cubic phase is predicted to remain metastable up to 1000 K, with an approximately constant free energy difference with respect to the *Pnma* phase. In contrast, the free energy of the rocksalt phase, computed under the same assumptions as for the *Cmcm* phase, falls with temperature, but remains above the *Pnma* phase in energy across the range of temperatures considered.

Finally, we also consider the effect of vibrational contributions to the free energy on the stability of Sn₂S₃. Figure 6 compares the temperature dependence of the free energy, ΔA , of the disproportionation reaction:



In light of the free-energy crossing evident in Figure 5, we consider decomposition to both *Pnma* and *Cmcm* SnS. The calculated reaction energies at representative temperatures are given in Table 5.

PBEsol and PBEsol + D3 both predict the decomposition to the *Pnma* phase to become less favourable with temperature (i.e. the free energy increases), whereas decomposition to the *Cmcm* phase becomes more favourable (i.e. the energy decreases). The PBEsol free energies predict decomposition to the *Pnma* phase to become unfavourable above ~650 K; however, decomposition to the *Cmcm* phase is a lower-energy pathway above ~400 K, and the reaction remains favourable.

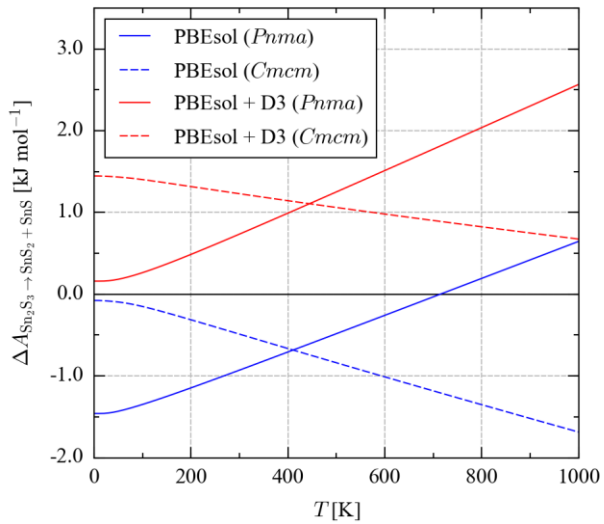


Figure 6 Constant-volume (Helmholtz) free energy, A , for the decomposition of Sn_2S_3 into SnS_2 and SnS as a function of temperature, calculated with PBEsol (blue) and PBEsol + D3 (red). Based on the stability ordering of the SnS phases (Figures 2/5, Tables 3/4), we consider decomposition to both the *Pnma* (solid lines) and *Cmcm* (dashed lines) phases of SnS .

	[kJ mol ⁻¹ Per F.U.]	
	PBEsol	PBEsol + D3
ΔU_{latt}	-1.68	-0.14
$\Delta A_{0\text{K}}$	-1.51	0.12
$\Delta A_{300\text{K}}$	-0.98	0.69
$\Delta A_{900\text{K}}$	0.37	2.26
<i>Cmcm</i> SnS : $\Delta A_{900\text{K}}$	-1.57	0.71

Table 5 Reaction energies for the decomposition reaction $\text{Sn}_2\text{S}_3 \rightarrow \text{SnS}_2 + \text{SnS}$, calculated based on the differences in the athermal lattice energies (ΔU_{latt}) and the constant-volume (Helmholtz) free energies (ΔA) at 0, 300 and 900 K. A negative energy implies that Sn_2S_3 is unstable, while a positive energy indicates the reverse. The energies are given with respect to *Pnma* SnS , as this was determined to be the energetic ground-state, while the 900 K free energy calculated with respect to the *Cmcm* phase, which has the lowest free energy of the SnS phases above ~ 400 K, is also given.

With PBEsol + D3, on the other hand, the inclusion of zero-point energy renders decomposition unfavourable at 0 K, and it remains so up to 1000 K.

Given the theoretical reports predicting Sn_2S_3 to be unstable with respect to *Pnma* SnS and SnS_2 , it is of interest to ascertain whether this result can also be obtained with other dispersion correction methods. We therefore performed calculations on *Pnma* and *Cmcm* SnS, SnS_2 and Sn_2S_3 with the newer variant of PBEsol + D3 with the Beck-Johnson damping scheme⁵² (see Table S2 and Figures S3/S4 in the supporting information). These calculations yielded the same qualitative result, i.e. that the dispersion correction brings Sn_2S_3 closer to the convex hull than uncorrected PBEsol, and the subsequent inclusion of the vibrational contributions to the free energy predicts it to be thermodynamically stable up to 1000 K. Although the Becke-Johnson-damped DFT-D3 is similar to the “bare” D3, we note that the majority of the other well-known dispersion corrections, e.g. DFT-D2,⁵³ the Tkatchenko-Scheffler method (DFT-TS),⁵⁴ and the more sophisticated many-body dispersion technique,^{55,56} do not have scaling constants optimised for PBEsol. To investigate other common dispersion corrections would thus also require the exploration of other GGA functionals, which we defer to a future study.

Although, as noted above regarding the predicted *Pnma*-to-*Cmcm* phase-transition temperature, these calculations may still be missing some important effects, the predicted stability of Sn_2S_3 with PBEsol + D3 is in keeping with experimental findings. These results therefore highlight the potential importance of both a sufficient description of dispersion interactions and of vibrational contributions to the free energy in assessing the phase stability of the tin sulfides.

Conclusions

In summary, this work has provided detailed insight into the thermodynamic and dynamical stability of the seven currently known and proposed compounds in the Sn_xS_y phase space, addressing several key outstanding questions.

The recently-discovered π -cubic phase is metastable with respect to the orthorhombic *Pnma/Cmcm* equilibrium. The bulk rocksalt phase is higher in energy and is dynamically unstable, but could potentially be stabilised under pressure or epitaxial strain. Our calculations show conclusively that the hypothetical zincblende phase is both energetically and dynamically unstable, and we suggest that reports of this phase be reassessed as either of the other two cubic phases.

Finally, we also show that accurately modelling the tin sulfide phase diagram, in particular reproducing the experimentally-observed stability of the sesquisulfide, may require theoretical techniques which afford a good treatment of dispersion interactions, and possibly also the inclusion of contributions to the energetics from lattice dynamics. This result provides a baseline for further theoretical characterisation of this less-well-studied tin sulfide phase.

Electronic supporting information

Electronic supporting information includes formation energies and a convex hull calculated with reference to α -SnS, volume-dependent phonon dispersions for rocksalt and zincblende SnS calculated with the PBEsol functional, optimised lattice parameters and phonon dispersions of *Pnma* and *Cmcm* SnS, SnS₂ and Sn₂S₃ calculated with PBEsol + D3 (BJ), and the calculated temperature-dependent Helmholtz free energy of decomposition of Sn₂S₃ obtained with PBEsol + D3 (BJ).

Data-access statement

The data from these calculations, including the optimised structures, force constants, phonon dispersions and density of states curves, and thermodynamic functions, are available in an online repository at <https://doi.org/10.15125/BATH-00339> (see also <https://github.com/WMD-group/Phonons>).

Acknowledgements

JMS gratefully acknowledges support from an EPSRC Programme Grant (grant no. EP/K004956/1). LAB is an International Research Fellow of the Japan Society of Promotion of Science (JSPS; grant no. 26.04792). AW acknowledges support from the Royal Society and the ERC (grant no. 277757). Calculations were carried out using the SiSu supercomputer at the IT Center for Science (CSC), Finland, via the Partnership for Advanced Computing in Europe (PRACE) project no. 13DECI0317/IsoSwitch, and on the Balena HPC cluster at the University of Bath, which is maintained by Bath University Computing Services. Some of the calculations were also carried out on the UK national Archer HPC facility, accessed through membership of the UK Materials Chemistry Consortium, which is funded by EPSRC grant no. EP/L000202.

References

1. Noguchi, H.; Setiyadi, A.; Tanamura, H.; Nagatomo, T.; Omoto, O., Characterization of vacuum-evaporated tin sulfide film for solar cell materials. *Sol. Energ. Mat. Sol. C* **1994**, *35*, 325-331.
2. Reddy, K. T. R.; Reddy, N. K.; Miles, R. W., Photovoltaic properties of SnS based solar cells. *Sol. Energ. Mat. Sol. C* **2006**, *90*, 3041-3046.
3. Sinsermsuksakul, P.; Sun, L.; Lee, S. W.; Park, H. H.; Kim, S. B.; Yang, C.; Gordon, R. G., Overcoming efficiency limitations of SnS-based solar cells. *Adv. Energy Mater.* **2014**, *4*, 1400496.
4. Shen, J.; He, Y.; Wu, J.; Gao, C.; Keyshar, K.; Zhang, X.; Yang, Y.; Ye, M.; Vajtai, R.; Lou, J.; Ajayan, P. M., Liquid phase exfoliation of two-dimensional materials by directly probing and matching surface tension components. *Nano Lett.* **2015**, *15*, 5449-5454.
5. Burton, L. A.; Walsh, A., Phase stability of the earth-abundant tin sulfides SnS, SnS₂, and Sn₂S₃. *J. of Phys. Chem. C* **2012**, *116*, 24262-24267.
6. Kumagai, Y.; Burton, L. A.; Walsh, A.; Oba, F., Electronic structure and defect physics of tin sulfides: SnS, Sn₂S₃, and SnS₂. *Phys. Rev. Appl.* **2016**, *6*, 014009.
7. Albers, W.; Haas, C.; Vink, H. J.; Wasscher, J. D., Investigations on SnS. *J. Appl. Phys.* **1961**, *32*, 2220-2225.
8. Hofmann, W., Ergebnisse der strukturbestimmung komplexer sulfide. *Z. Kristallogr.* **1935**, *92*, 161-185.
9. Vonschnering, H. G.; Wiedemeier, H., The high-temperature structure of beta-Sns and beta-SnSe and the B16-to-B33 type Lambda-transition path. *Z. Kristallogr.* **1981**, *156*, 143-150.
10. Mariano, A. N.; Chopra, K. L., Polymorphism in some IV-VI compounds induced by high pressure and thin-film epitaxial growth. *Appl. Phys. Lett.* **1967**, *10*, 282-284.
11. Greyson, E. C.; Barton, J. E.; Odom, T. W., Tetrahedral zinc blende tin sulfide nano- and microcrystals. *Small* **2006**, *2*, 368-371.
12. Avellaneda, D.; Nair, M. T. S.; Nair, P. K., Polymorphic tin sulfide thin films of zinc blende and orthorhombic structures by chemical deposition. *J. Electrochem. Soc.* **2008**, *155*, D517-D525.

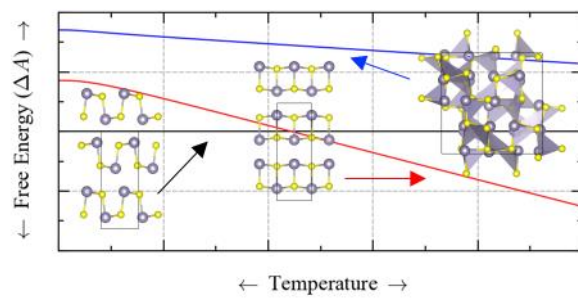
13. Ahmet, I. Y.; Hill, M. S.; Johnson, A. L.; Peter, L. M., Polymorph-selective deposition of high purity SnS thin films from a single source precursor. *Chem. Mater.* **2015**, *27*, 7680- 7688.
14. Rabkin, A.; Samuha, S.; Abutbul, R. E.; Ezersky, V.; Meshi, L.; Golan, Y., New nanocrystalline materials: a previously unknown simple cubic phase in the SnS binary system. *Nano Lett.* **2015**, *15*, 2174-2179.
15. Abutbul, R. E.; Garcia Angelmo, A. R.; Burshtein, Z.; Nair, M. T. S.; Nair, P. K.; Golan, Y., Crystal structure of a large cubic tin mono-sulfide polymorph: An unraveled puzzle. *CrystEngComm* **2016**, *18*, 5188-5194.
16. Abutbul, R. E.; Segev, E.; Zeiri, L.; Ezersky, V.; Makov, G.; Golan, Y., Synthesis and properties of nanocrystalline π -SnS - a new cubic phase of tin sulphide. *RSC Adv.* **2016**, *6*, 5848-5855.
17. Garcia-Angelmo, A. R.; Romano-Trujillo, R.; Campos-Álvarez, J.; Gomez-Daza, O.; Nair, M. T. S.; Nair, P. K., Thin film solar cell of SnS absorber with cubic crystalline structure. *Phys. Status Solidi (a)* **2015**, *212*, 2332-2340.
18. Burton, L. A.; Colombara, D.; Abellon, R. D.; Grozema, F. C.; Peter, L. M.; Savenije, T. J.; Dennler, G.; Walsh, A., Synthesis, characterization, and electronic structure of single-crystal SnS, Sn₂S₃, and SnS₂. *Chem. Mater.* **2013**, *25*, 4908-4916.
19. Jain, A.; Ong, S. P.; Hautier, G.; Chen, W.; Richards, W. D.; Dacek, S.; Cholia, S.; Gunter, D.; Skinner, D.; Ceder, G.; Persson, K. A., Commentary: the Materials Project: A materials genome approach to accelerating materials innovation. *APL Mater.* **2013**, *1*, 011002.
20. Persson, K. Materials Data on Sn₂S₃ (SG:62) by Materials Project.
<https://materialsproject.org/materials/mp-1509/> (accessed 2016-07-28).
21. Whittles, T. J.; Burton, L. A.; Skelton, J. M.; Walsh, A.; Veal, T. D.; Dhanak, V. R., Band alignments, valence bands and core levels in the tin sulfides SnS, SnS₂ and Sn₂S₃: Experiment and theory. *Chem. Mater.* **2016**, *28*, 2718-3726.
22. Scragg, J. J.; Watjen, J. T.; Edoff, M.; Ericson, T.; Kubart, T.; Platzer-Bjorkman, C., A detrimental reaction at the molybdenum back contact in Cu₂ZnSn(S,Se)₄ thin-film solar cells. *J. Am. Chem. Soc.* **2012**, *134*, 19330-19333.
23. Hohenberg, P.; Kohn, W., Inhomogenous electron gas. *Phys. Rev.* **1964**, *136*, B864-B871.

24. Kohn, W.; Sham, L. J., Self-consistent equations including exchange and correlation effects. *Phys. Rev.* **1965**, *140*, A1133-A1138.
25. Burton, L. A.; Whittles, T. J.; Hesp, D.; Linhart, W. M.; Skelton, J. M.; Hou, B.; Webster, R. F.; O'Dowd, G.; Reece, C.; Cherns, D.; *et al.*, Electronic and optical properties of single crystal SnS₂: An earth-abundant disulfide photocatalyst. *J. Mater. Chem. A* **2016**, *4*, 1312-1318.
26. Skelton, J. M.; Parker, S. C.; Togo, A.; Tanaka, I.; Walsh, A., Thermal physics of the lead chalcogenides PbS, PbSe, and PbTe from first principles. *Phys. Rev. B* **2014**, *89*, 205203.
27. da Silva, E. L.; Skelton, J. M.; Parker, S. C.; Walsh, A., Phase stability and transformations in the halide perovskite CsSnI₃. *Phys. Rev. B* **2015**, *91*, 144107.
28. Perdew, J. P.; Ruzsinszky, A.; Csonka, G. I.; Vydrov, O. A.; Scuseria, G. E.; Constantin, L. A.; Zhou, X. L.; Burke, K., Restoring the density-gradient expansion for exchange in solids and surfaces. *Physical Review Letters* **2008**, *100*, 136406.
29. Grimme, S.; Antony, J.; Ehrlich, S.; Krieg, H., A consistent and accurate *ab initio* parametrization of density functional dispersion correction (DFT-D) for the 94 elements H-Pu. *J. Chem. Phys.* **2010**, *132*, 154104.
30. Kresse, G.; Hafner, J., *Ab initio* molecular dynamics for liquid metals. *Phys. Rev. B* **1993**, *47*, 558(R)-561(R).
31. He, L.; Liu, F.; Hautier, G.; Oliveira, M. J. T.; Marques, M. A. L.; Vila, F. D.; Rehr, J. J.; Rignanese, G. M.; Zhou, A., Accuracy of generalized gradient approximation functionals for density-functional perturbation theory calculations. *Phys. Rev. B* **2014**, *89*, 064305.
32. Skelton, J. M.; Tiana, D.; Parker, S. C.; Togo, A.; Tanaka, I.; Walsh, A., Influence of the exchange-correlation functional on the quasi-harmonic lattice dynamics of II-VI semiconductors. *J. Chem. Phys.* **2015**, *143*, 064710.
33. Charles, N.; Rondinelli, J. M., Assessing exchange-correlation functional performance for structure and property predictions of oxyfluoride compounds from first principles. *Phys. Rev. B* **2016**, *94*, 174108.
34. Abrahams, S., The crystal and molecular structure of orthorhombic sulfur. *Acta Crystallogr.* **1955**, *8*, 661-671.

35. Wyckoff, R. W. G., *Crystal Structures Vol. 1*, 2nd ed.; Wiley: New York, 1963.
36. Hazen, R. M.; Finger, L. W., The crystal structures and compressibilities of layer minerals at high pressure. *Am. Mineral.* **1978**, *63*, 289-292.
37. Kniep, R.; Mootz, D.; Severin, U.; Wunderlich, H., Structure of tin(II) tin(IV) trisulphide, a redetermination. *Acta Crystallogr. Sect. B* **1982**, *38*, 2022-2023.
38. Blochl, P. E., Projector augmented-wave method. *Phys. Rev. B* **1994**, *50*, 17953-17979.
39. Kresse, G.; Joubert, D., From ultrasoft pseudopotentials to the projector augmented-wave method. *Phys. Rev. B* **1999**, *59*, 1758-1775.
40. Monkhorst, H. J.; Pack, J. D., Special points for Brillouin-zone integrations. *Phys. Rev. B* **1976**, *13*, 5188-5192.
41. Togo, A.; Oba, F.; Tanaka, I., First-principles calculations of the ferroelastic transition between rutile-type and CaCl₂-type SiO₂ at high pressures. *Phys. Rev. B* **2008**, *78*, 134106.
42. Togo, A.; Tanaka, I., First principles phonon calculations in materials science. *Scr. Mater.* **2015**, *108*, 1-5.
43. Parlinski, K.; Li, Z. Q.; Kawazoe, Y., First-principles determination of the soft mode in cubic ZrO₂. *Phys. Rev. Lett.* **1997**, *78*, 4063-4066.
44. Momma, K.; Izumi, F., VESTA 3 for three-dimensional visualization of crystal, volumetric and morphology data. *J. of Appl. Crystallogr.* **2011**, *44*, 1272-1276.
45. Nasirov, V. I.; Adgezalova, K. A., Stabilization of low-temperature SnS by rare-earth doping. *Inorg. Mater.* **2001**, *37*, 1099-1100.
46. Walsh, A.; Watson, G. W., Influence of the anion on lone pair formation in Sn(II) monochalcogenides: a DFT study. *J. Phys. Chem. B* **2005**, *109*, 18868-18875.
47. *CRC Handbook of Chemistry and Physics*, 97th ed.; CRC Press: Boca Raton, FL, 2016.
48. Sharma, R. C.; Chang, Y. A., The S-Sn (sulfur-tin) system. *Bull. Alloy Phase Diagr.* **1986**, *7*, 269-273.
49. Novoselova, A. V.; Zlomanov, V. P.; Karbanov, S. G.; Matveyev, O. V.; Gas'kov, A. M., Physico-chemical study of the germanium, tin, lead chalcogenides. *Prog. Solid State Ch.* **1972**, *7*, 85-115.

50. Piacente, V.; Foglia, S.; Scardala, P., Sublimation study of the tin sulfides SnS_2 , Sn_2S_3 and SnS . *J. Alloys Compd.* **1991**, *177*, 17-30.
51. Skelton, J. M.; Burton, L. A.; Parker, S. C.; Walsh, A.; Kim, C.-E.; Soon, A.; Buckeridge, J.; Sokol, A. A.; Catlow, C. R. A.; Togo, A.; Tanaka, I., Anharmonicity in the high-temperature *Cmcm* phase of SnSe: Soft modes and three-phonon interactions. *Phys. Rev. Lett.* **2016**, *117*, 075502.
52. Grimme, S.; Ehrlich, S.; Goerigk, L., Effect of the damping function in dispersion corrected density functional theory. *J. Comput. Chem.* **2011**, *32*, 1456-1465.
53. Grimme, S., Semiempirical GGA-type density functional constructed with a long-range dispersion correction. *J. Comput. Chem.* **2006**, *27*, 1787-1799.
54. Tkatchenko, A.; Scheffler, M., Accurate molecular van der Waals interactions from ground-state electron density and free-atom reference data. *Phys. Rev. Lett.* **2009**, *102*, 073005.
55. Tkatchenko, A.; DiStasio, R. A.; Car, R.; Scheffler, M., Accurate and efficient method for many-body van der Waals interactions. *Phys. Rev. Lett.* **2012**, *108*, 236402.
56. Ambrosetti, A.; Reilly, A. M.; DiStasio, R. A. Jr.; Tkatchenko, A., Long-range correlation energy calculated from coupled atomic response functions. *J. Chem. Phys.* **2014**, *140*, 18A508.

TOC Graphic



Supporting Information:

Chemical and Lattice Stability of the Tin Sulfides

Jonathan M. Skelton,^{1*} Lee A. Burton,² Fumiyasu Oba,² and Aron Walsh^{1,3,4}

¹ Department of Chemistry, University of Bath, Claverton Down, Bath BA2 7AY, UK

² Laboratory for Materials and Structures, Institute of Innovative Research, Tokyo Institute of Technology, 4259 Nagatsuta, Midori-ku, Yokohama 226-8503, Japan

³ Department of Materials, Imperial College London, Exhibition Road, London SW7 2AZ, UK

⁴ Global E³ Institute and Department of Materials Science and Engineering, Yonsei University, Seoul 120-749, Korea

* Corresponding author; e-mail: j.m.skelton@bath.ac.uk

System	E_F [kJ mol ⁻¹ per F.U.]		
	PBEsol	PBEsol + D3	Expt.
SnS (<i>Pnma</i>)	-93.04	-98.93	-100 to -108 ^{1,2}
SnS (π -cubic)	-90.85	-96.39	-
SnS (<i>Cmcm</i>)	-91.29	-97.29	-
SnS (Rocksalt)	-84.50	-88.17	-
SnS (Zincblende)	-20.81	-18.37	-
SnS ₂	-122.45	-131.40	-148 to -182 ^{2,4}
Sn ₂ S ₃	-213.81	-230.18	-249 to -297 ^{2,4}

Table S1 Formation energies (E_F) of the *Pnma*, π -cubic, *Cmcm*, rocksalt and zincblende phases of SnS, SnS₂ and Sn₂S₃, calculated with reference to α -Sn. These may be compared to the data in Table 3 in the text. Experimental values are given where available for comparison.

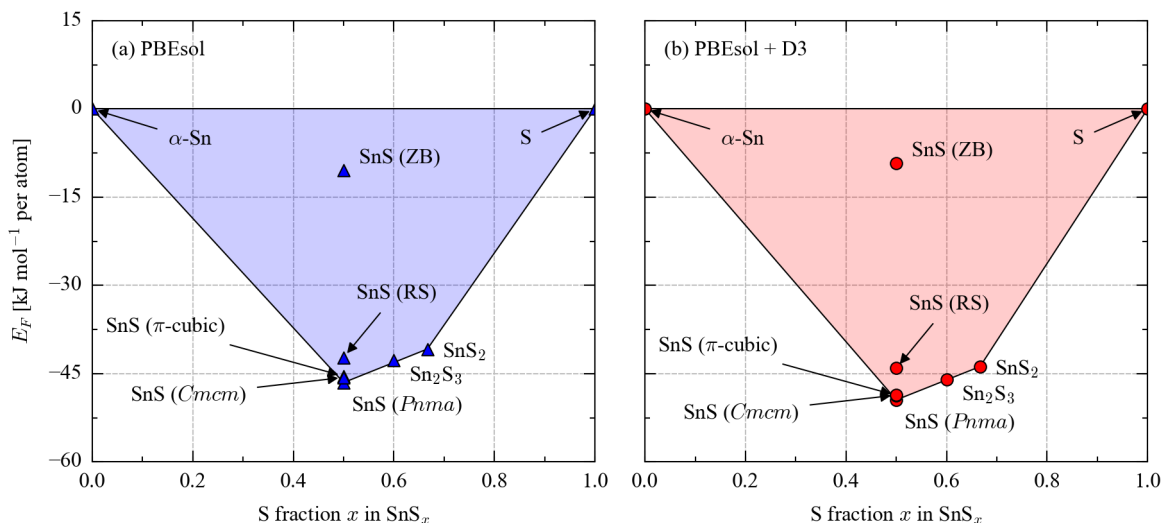


Figure S1 Convex hulls calculated for the Sn_xS_y system, based on the formation energies in Table S1 (i.e. referenced to α -Sn) obtained with (a) PBEsol and (b) PBEsol + D3. These may be compared to the convex hulls presented in Figure 2 in the text.

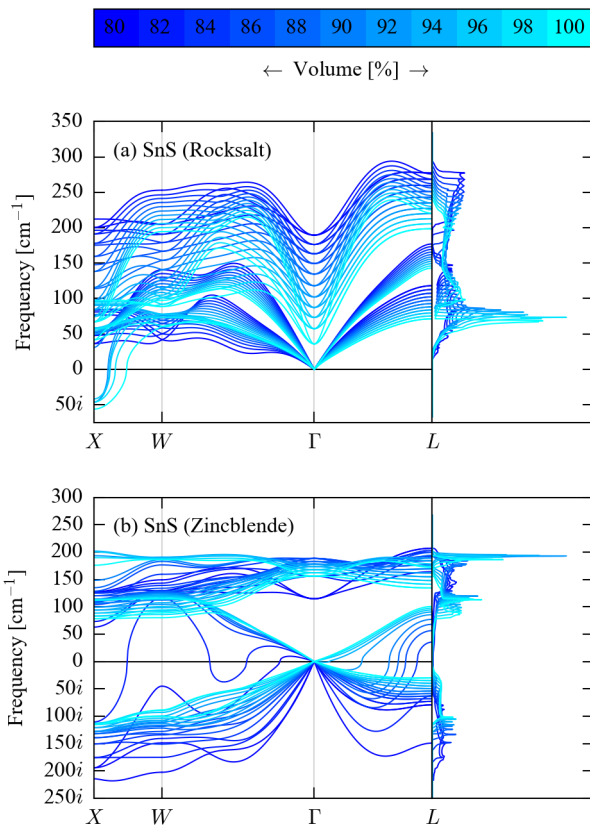


Figure S2 Phonon dispersion and density of states curves for the rocksalt (a) and zincblende (b) phases of SnS calculated at cell volumes ranging from the athermal equilibrium (cyan) to a 20 % compression (blue). Both sets of curves were computed with PBEsol, and may be compared to the corresponding plots in Figure 4 in the text.

	PBEsol			PBEsol + D3			PBEsol + D3 (BJ)			Expt.	
	<i>a</i> [Å]	<i>b</i> [Å]	<i>c</i> [Å]	<i>a</i> [Å]	<i>b</i> [Å]	<i>c</i> [Å]	<i>a</i> [Å]	<i>b</i> [Å]	<i>c</i> [Å]	<i>a</i> [Å]	<i>b</i> [Å]
SnS (<i>Pnma</i>)	4.250	11.082	3.978	4.220	10.976	3.958	4.113	10.887	3.953	4.33 ⁵	11.18 ⁵
SnS (<i>Cmcm</i>) ^a	4.037	11.282	4.039	4.018	11.186	4.009	3.987	11.005	3.988	4.148 ⁶	11.480 ⁶
SnS ₂	3.651	-	6.015	3.639	-	5.721	3.625	-	5.584	3.638 ⁷	-
Sn ₂ S ₃	8.811	3.766	13.813	8.633	3.760	13.663	8.420	3.754	13.532	8.878 ⁸	3.751 ⁸
											14.020 ⁸

Table S2 Lattice parameters of *Pnma* and *Cmcm* SnS, SnS₂ and Sn₂S₃ obtained with the PBEsol, PBEsol + D3 and PBEsol + D3 (BJ) exchange-correlation functionals. The PBEsol and PBEsol + D3 values data are reproduced from Table 2 in the text for comparison. Experimental values are also given for comparison. ^aThe lattice constants in Ref. 6 are reported at 905 K, and are therefore expected to include significant thermal expansion.

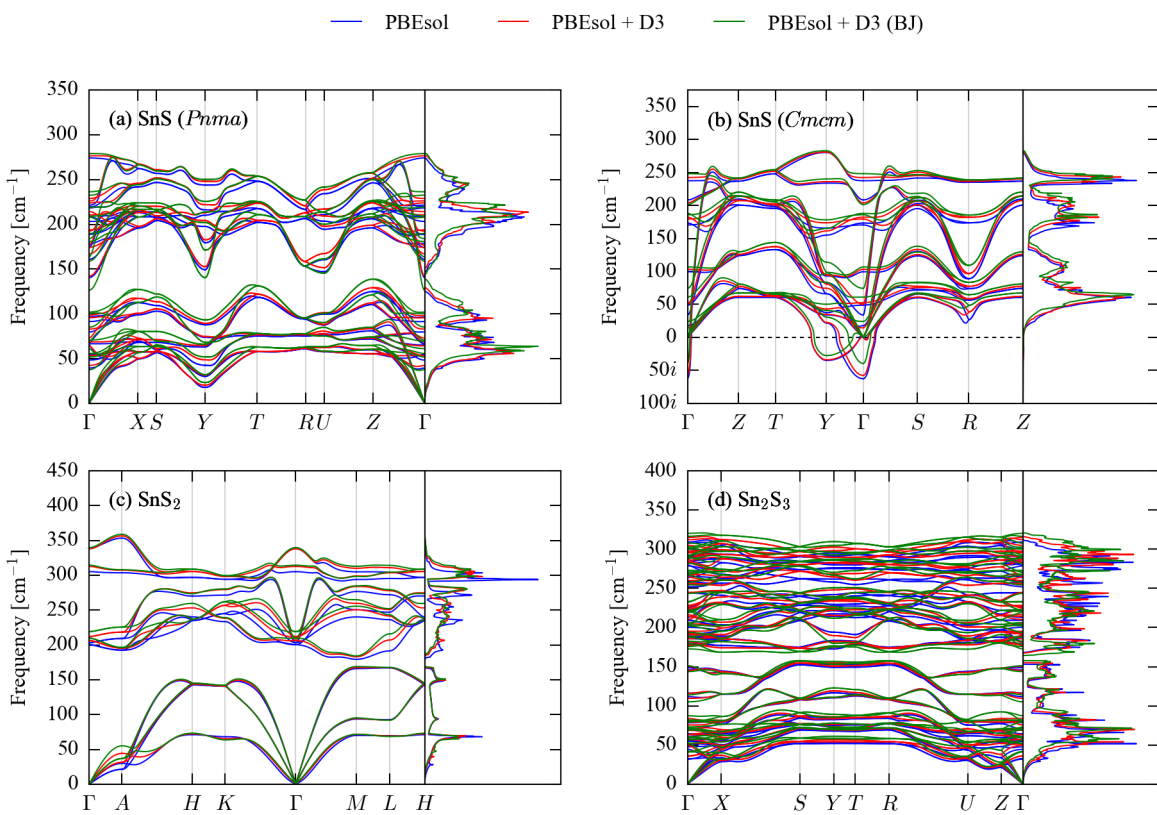


Figure S3 Phonon dispersion and density of states curves for *Pnma* (a) and *Cmcm* (b) SnS, SnS₂ (c) and Sn₂S₃ (d), calculated using the PBEsol (blue), PBEsol + D3 (red) and PBEsol + D3 (BJ) (green) functionals. The PBEsol and PBEsol + D3 data are duplicated from the relevant subplots of Figure 3 in the text for comparison.

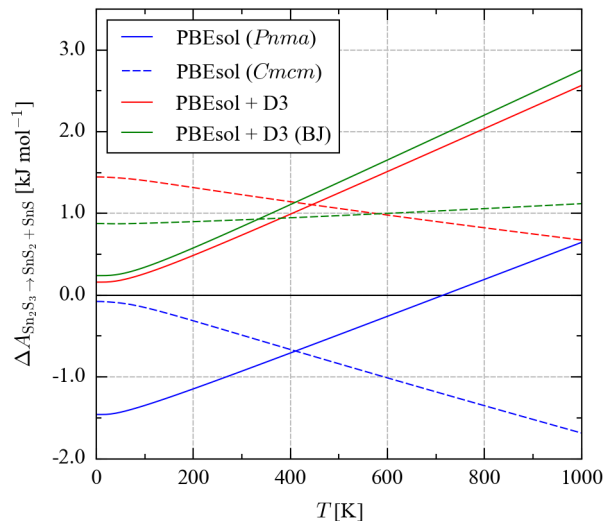


Figure S4 Constant-volume (Helmholtz) free energy for the decomposition reaction $\text{Sn}_2\text{S}_3 \rightarrow \text{SnS}_2 + \text{SnS}$ as a function of temperature, calculated with PBEsol (blue), PBEsol + D3 (red) and PBEsol + D3 (BJ) (green). Based on the stability ordering of the SnS phases (Figures 2/5 and Tables 3/4 in the text), we consider decomposition to both the *Pnma* (solid lines) and *Cmcm* (dashed lines) phases of SnS.

References

1. CRC Handbook of Chemistry and Physics, 97th ed.; CRC Press: Boca Raton, FL, 2016.
2. Sharma, R. C.; Chang, Y. A., The S–Sn (sulfur-tin) system. *Bull. Alloy Phase Diagr.* **1986**, *7*, 269–273.
3. Novoselova, A. V.; Zlomanov, V. P.; Karbanov, S. G.; Matveyev, O. V.; Gas'kov, A. M., Physico-chemical study of the germanium, tin, lead chalcogenides. *Prog. Solid State Ch.* **1972**, *7*, 85–115.
4. Piacente, V.; Foglia, S.; Scardala, P., Sublimation study of the tin sulfides SnS_2 , Sn_2S_3 and SnS . *J. Alloys Compd.* **1991**, *177*, 17–30.
5. Hofmann, W., Ergebnisse der strukturbestimmung komplexer sulfide. *Z. Kristallogr.* **1935**, *92*, 161–185.
6. Vonschnerring, H. G.; Wiedemeier, H., The high-temperature structure of beta-Sns and beta-SnSe and the B16-to-B33 type Lambda-transition path. *Z. Kristallogr.* **1981**, *156*, 143–150.
7. Hazen, R. M.; Finger, L. W., The crystal structures and compressibilities of layer minerals at high pressure. *Am. Mineral.* **1978**, *63*, 289–292.
8. Kniep, R.; Mootz, D.; Severin, U.; Wunderlich, H., Structure of tin(II) tin(IV) trisulphide, a redetermination. *Acta Crystallogr. Sect. B* **1982**, *38*, 2022–2023.